# Thickness of the rim of an expanding lamella near the splash threshold

Jolet de Ruiter,[1,a)] Rachel E. Pepper,[2,b)] and Howard A. Stone[3,c)]
[1]*Food Process Engineering Group, Wageningen University, 6703 HD Wageningen, The Netherlands*
[2]*Department of Physics, Harvard University, Cambridge, Massachusetts 02138, USA*
[3]*School of Engineering and Applied Sciences, Harvard University, Cambridge, Massachusetts 02138, USA*

(Received 5 May 2009; accepted 22 December 2009; published online 24 February 2010)

The evolution of the ejected liquid sheet, or lamella, created after impact of a liquid drop onto a solid surface is studied using high-speed video in order to observe the detailed time evolution of the thickness of the rim of the lamella. Since it has been suggested that splashing behavior is set at very early times after impact, we study early times up to $D_0/U_0$, where $D_0$ and $U_0$ are the diameter and speed of the impacting drop, respectively, for different liquid viscosities and impact speeds below the splashing threshold. Within the regime of our experiments, our results are not consistent with the idea that the lamella rim grows similar to the boundary layer thickness. Rather, we find that the rim thickness is always much larger than the boundary layer thickness, and that the rim thickness decreases with increasing impact speed. For lower impact speeds, the increase in the rim thickness is consistent with a $\sqrt{t}$ response over the limited time range available, but the dependence is not simply proportional to $\sqrt{\nu}$, where $\nu$ is the kinematic viscosity, and there is a strong dependence of the rim thickness on the impact speed $U_0$. Scaling of the rim height using a balance of inertial and surface tension forces provides some collapse of the data at lower impact speeds. We also observe an unusual plateau behavior in thickness versus time at higher impact speeds as we approach the splash threshold. © *2010 American Institute of Physics*. [doi:10.1063/1.3313360]

## I. INTRODUCTION

Liquid drop impacts on solid substrates and the resulting spread and splash are important in a range of industrial and agricultural applications including spray coating and cooling,[1] ink-jet printing,[2,3] fuel combustion,[4] and pesticide delivery.[5,6] Splashing has been extensively studied experimentally, theoretically, and computationally (see Ref. 7 for a recent review). However, the mechanism of splashing is not yet fully understood.

An understanding of the time dependence of the thickness of the expanding liquid sheet, or lamella, generated after droplet impact is of fundamental importance for quantitatively describing both the spreading and splashing after impact. A full understanding would include the evolution of the entire lamella profile including the inner portion and the rim. It is common in recent theories of splashing to assume that the lamella thickness is proportional to the thickness, $\sqrt{\nu t}$, of a viscous boundary layer, where $\nu$ is the kinematic viscosity of the liquid and $t$ is the time after impact.[8–12] This same idea has also been used for film thickness after impact on a thin liquid film.[13] A functional form for the lamella thickness is also essential for theories of film spreading after droplet impact.[14–17] Recently, numerical studies of this topic have appeared.[18–20] In this paper we report detailed measurements of the time-dependent thickness of the rim of the lamella, based on side-view profiles of the drop shape.

A feature of the development of the expanding lamella that is frequently neglected is the formation of a thickened rim around the edge, as in Fig. 1(b). For example, only occasionally in literature is the thickness of the inner lamella, $h_L$, distinguished from the thickness of the rim, $h_R$.[21,22] In one such study, Roisman *et al.*[21] considered an average lamella thickness at times earlier than the characteristic time, $D_0/U_0$, where $D_0$ and $U_0$ are the diameter and impact velocity of the drop, respectively, while a second study of Attané *et al.*[22] was not valid in the regime relevant to splashing since near the splashing transition the thickened rim may move at a different speed than the fluid in the inner lamella. In theories of splashing, the thickness of the outermost portion of the lamella (furthest away from the point of impact in the radial direction) is the most relevant simply because that is the site of instability formation and growth,[23,24] from which secondary droplets may be emitted, both in prompt splashing[25] and for corona splashes at the splashing transition [see Fig. 1 of Ref. 9 and Fig. 3(a) of Ref. 26]. In both these cases, at the splashing transition, drops may be emitted after a rim has developed at the edge of the lamella [see Figs. 3(a) and 4 of Ref. 26]. Indeed, the thickness of this rim (once it develops) plays a critical role in both the splash threshold and droplet size for prompt splashes.[27] In some papers where a boundary layer time dependence is injected into a scaling argument (i.e., a thickness that grows proportional to $\sqrt{\nu t}$), the authors clearly refer to the outermost portion of the lamella which we interpret as the rim.[9] In other papers, the authors apparently refer interchangeably to the central part of the lamella and the curved end where surface tension acts.[8,10–12] For all of these cases, detailed experimental

[a)]Present address: Department of Science and Technology, University of Twente, 7500 AE Enschede, Netherlands.
[b)]Present address: Department of Physics, University of Colorado, Boulder, CO 80309.
[c)]Present address: Department of Mechanical and Aerospace Engineering, Princeton University, Princeton, NJ 08544.

 

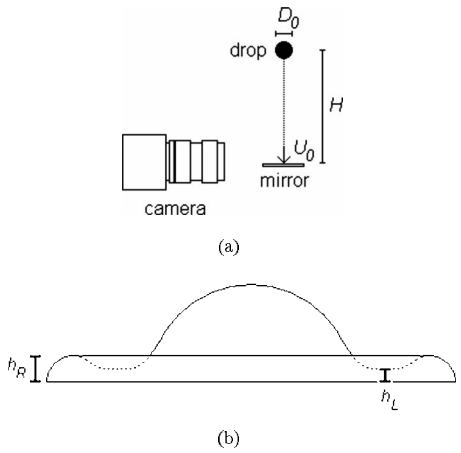


FIG. 1. (a) Schematic of the experimental setup (not to scale). The impact of a drop with diameter $D_0$, falling from a height $H$, with a resulting impact velocity $U_0$, is recorded with a high-speed camera aligned to take a side-view video of the impact. (b) Schematic of the distances measured: Due to radial expansion of the rim, the measured height represents the height of the rim (solid line), $h_R$, instead of the height of the inner portion of the lamella, $h_L$ (dotted line).

measurements of the rim thickness, which we report here, can be viewed as constraints on possible simplified models.

Despite the theoretical predictions and relevance of the lamella thickness to understanding both spreading and splashing phenomena, there have been relatively few direct measurements, particularly at the time scale relevant for splashing. Imaging the lamella experimentally in order to measure thickness is difficult, and the use of side views for imaging necessarily means that the thickest part of the lamella, the rim, is measured. For example, Stow and Hadfield[28] reported rim thickness versus time, but for only one impact experiment, and with four data points in the relevant time window $\mathcal{O}(D_0/U_0)$. Also, Roisman *et al.*[10] reported several measurements of the average lamella thickness at the time $D_0/U_0$; however these values are calculated from measurements of the lamella radius using volume conservation rather than measured directly. In their comprehensive paper about water spreading on glass, Roux and Cooper-White[29] reported the lamella rim thickness for several impact velocities. They concluded that the thickness grows approximately linearly with time and that the maximum thickness is a decreasing function of impact speed.[29] Although their relatively low spatial resolution makes it difficult to compare their results with theoretical predictions at times relevant for splashing, their data do suggest that the rim is too thick for a simple $\sqrt{\nu t}$ thickness evolution to be valid.

Mongruel *et al.*[30] used high-speed imaging methods to measure the thickness of the lamella at times before a rim has developed (typically $t \leq 0.3 D_0/U_0$) and found that the height of both the base and tip of the lamella grow linearly in time. We have been unable to find any previous detailed experimental observations of the lamella rim thickness with both high spatial and temporal resolution. It is the purpose of this paper to provide, for several different fluid systems, quantitative data on the time evolution of the lamella rim thickness.

TABLE I. Physical properties of the alcohols used.

| Alcohol | $\mu$ ($\times 10^{-3}$ Pa s) [a] | $\rho$ (kg/m$^3$) [a] | $\gamma$ ($\times 10^{-3}$ N/m) [b] |
|---|---|---|---|
| Methanol | 0.55 | 786 | 23.2 |
| Ethanol | 1.08 | 785 | 22.2 |
| Isopropanol | 2.05 | 781 | 21.7 |

[a] $\mu$ is the shear viscosity at 25 °C (Ref. 32).
[b] $\rho$ is the density at 20 °C (Ref. 33).

It has been suggested that it is times very early after impact that determine splashing behavior.[26,31] We therefore measure for different liquid viscosities and drop impact speeds the evolution of the thickness of the rim of the lamella at times earlier than $D_0/U_0$. We choose impact speeds that range up to when instabilities form in the lamella. Our results are inconsistent with the simple idea that the rim thickness evolves proportional to a boundary layer thickness, $\sqrt{\nu t}$. Instead, we find two distinct behaviors: For slower impact speeds we find that the thickness increases monotonically with time, which is consistent with a $\sqrt{t}$ growth but find the thickness also strongly depends on impact speed, while for increased impact speeds we observe a plateau behavior in the lamella thickness versus time.

## II. EXPERIMENTAL METHODS

A schematic of the experimental setup is shown in Fig. 1(a). Millimeter-radius drops are released above a mirror, and their impacts are observed using a Phantom high-speed video camera recording at 57 971 frames/s. The spatial distance between a pair of pixels is about 27 $\mu$m. The drops impact onto a horizontally positioned mirror (Anchor Optics experimental grade first surface mirror), and the high-speed camera is carefully aligned with the mirror to obtain a side-view recording of the impacting droplet. Drops of reproducible diameter ($D_0 = 2.02 \pm 0.04$ mm) are generated using a syringe pump to create a pendant drop hanging below a needle of fixed inner diameter. The drop falls under its own weight. By adjusting the height of release, $H$, the impact velocity, $U_0$, is varied within the range of 0.90–1.71 m/s, hence a typical time $D_0/U_0 \approx 1.2$–$2.2$ ms. We analyze only impacts for which the lamella has a uniform rim height. Therefore, the highest impact speeds that we assess are just below the threshold for instabilities in the lamella, which, for ethanol, is slightly below the threshold for splashing of $1.91 \pm 0.08$ m/s (when detachment of satellite droplets first occurs). The viscosity of the drop is varied by using three different alcohols: methanol, ethanol, and isopropanol (Table I). The densities ($\rho$) and surface tensions ($\gamma$) of these alcohols are essentially the same, allowing us to isolate the effect of viscosity, although we only span a change of a factor of 4.

The liquid parameters can be combined into two dimensionless groups, $\mathrm{Re} = \rho D_0 U_0/\mu$ and $\mathrm{We} = \rho D_0 U_0^2/\gamma$. The Reynolds number (Re) gives the ratio of inertial to viscous forces, while the Weber number (We) gives the ratio of inertial to surface tension forces. Our experiments focus on the regime $\mathrm{Re} \gg \mathrm{We} \gg 1$ with $730 < \mathrm{Re} < 3810$ and

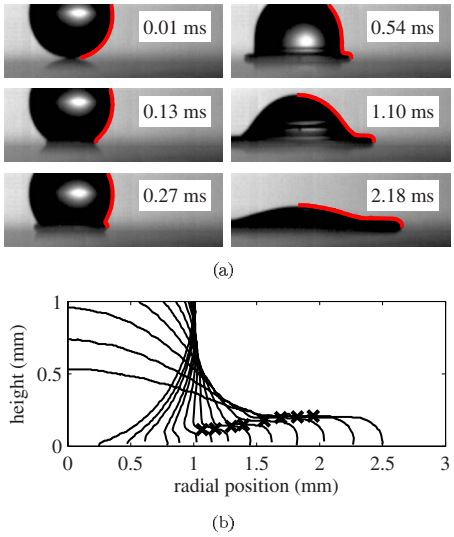


FIG. 2. (Color online) (a) Selection of frames from one typical high-speed video, taken up to a characteristic time $D_0/U_0$ (=2.18 ms) after impact (with speed $U_0$=0.93 m/s) of an ethanol drop ($D_0$=2.02 mm) onto a mirror. The reflection of the drop can be seen on the mirror. The time elapsed from impact is shown at the right of each frame. The time between sequential frames (not all are shown) is 0.017 ms. Thick gray lines (red online) show height profiles determined by our image-analysis software. (b) Height profiles of the impacting ethanol drop shown in (a). The height of the observed side-view profile is depicted as function of radial position for the right side of the recorded impacting drop. Fourteen frames are selected for analysis up to a time $D_0/U_0$ after impact, namely, at 0.004, 0.04, 0.06, 0.10, 0.12, 0.16, 0.20, 0.25, 0.32, 0.40, 0.50, 0.63, 0.79, and 1.00 times $D_0/U_0$. In time, the lamella expands radially. The crosses mark the location where the rim height of each profile is measured. Rim heights are only measured for profiles that show a plateau-shaped lamella.

$59<\mathrm{We}<185$. We report these dimensionless groups for ease of comparison with other experiments such as Refs. 29 and 30.

An example of a selection of frames from a high-speed video recording is shown in Fig. 2(a). The drop impact is analyzed up to a characteristic time $D_0/U_0$ after impact, which is the time in which a drop travels a distance equal to its diameter. We use custom-written MATLAB image-analysis software to determine the impact velocity, initial drop diameter, drop profile, and rim height, $h_R$, from the high-speed video recordings [see Fig. 1(b)]. To analyze the images, the pixels in each recorded frame are divided five times in both the horizontal and vertical directions into a total of 25 smaller pixels. Intensity values are assigned to these smaller pixels according to a bicubic interpolation of the surrounding intensity values. The spreading drop is identified by comparing the intensity of each (interpolated) pixel with a threshold intensity set by the background (nondrop) pixels. The height of the drop is determined at each radial position, taking into account the position of the surface of the mirror (determined from the drop and its reflection).

The drop profile is determined for a selection of frames after the moment of impact [see Fig. 2(b)]; the moment of impact ($t$=0) is defined midway between the frames just before and after impact. The rim heights are measured at the location of the plateau in the side-on view of the lamella [see x's in Fig. 2(b)]. At earlier times, the expelled sheet does not have a plateau, and an averaged thickness must be estimated [see Fig. 2(b) at times 0.10 and 0.12 $D_0/U_0$]. For times $<0.25D_0/U_0$, it is likely that the outermost portion of the lamella has not yet developed into a rim, so our measurements are of the thickness of the outermost portion of the lamella. We note that at these early instants, before the rim is formed, we measure a different portion of the lamella than what Mongrel *et al.*[30] did, so while our results are complementary, they are not directly comparable. Further, it should be emphasized that once the rim develops we measure the height of the rim—instead of the height of the inner lamella—since the rim obscures the inner portion of the lamella, as sketched in Fig. 1(b). Further examples of drop profiles after impact for different liquid/impact velocity combinations can be found in the Appendix.

The rim heights extracted from five independent experiments are averaged for each nondimensional time $t/(D_0/V_0)$. We confirmed that the error between two series (with similar conditions but performed on different days) of five repeated experiments is within the 95% confidence interval associated with one series.

## III. RESULTS AND DISCUSSION

### A. Drop impact observations

A typical series of high-speed images of the impact of an ethanol drop on a mirror is shown in Fig. 2(a). This series is representative of the quality of the recordings taken and the overall drop behavior observed during our experiments with different impact speeds and viscosities. Just after impact, a cylindrical foot is formed as the surface of the mirror is wetted by the ethanol drop [see Fig. 2(a) at 0.13 ms]. Shortly after, a liquid film, the lamella, is expelled from the leading edge of the drop [see Fig. 2(a) at 0.27 ms]. For impact speeds above 1.24 m/s (ethanol drops) a very thin lamella may be formed instantaneously, without first developing a foot. However due to the extremely short time scale and small dimension of the sheet, the existence of a distinct lamella at these times cannot be unambiguously established without more data at greater magnification. In any case, from our data, no influence of impact speed or liquid viscosity on the dimensionless time of the first appearance of the lamella could be identified. The lamella appears at a time of about $(0.072\pm0.04)D_0/U_0$ (95% confidence interval) for all conditions within the range of our experiments.

The lamella grows in both the radial direction and in height; see Fig. 2(a). The instant of the development of a thickened rim cannot be observed in the recording shown, as we see only the thickest part of the lamella in our side-on view. Recordings taken from a slight angle looking down on the drop (data not presented) show that a thickened rim appears at a time of $(0.25\pm0.03)D_0/U_0$. Truncated spherical shapes and stairlike capillary waves, as reported by Roux and Cooper-White,[29] were not observed since our impact speeds are, in general, outside the range in which stairlike capillary waves can develop.[34]

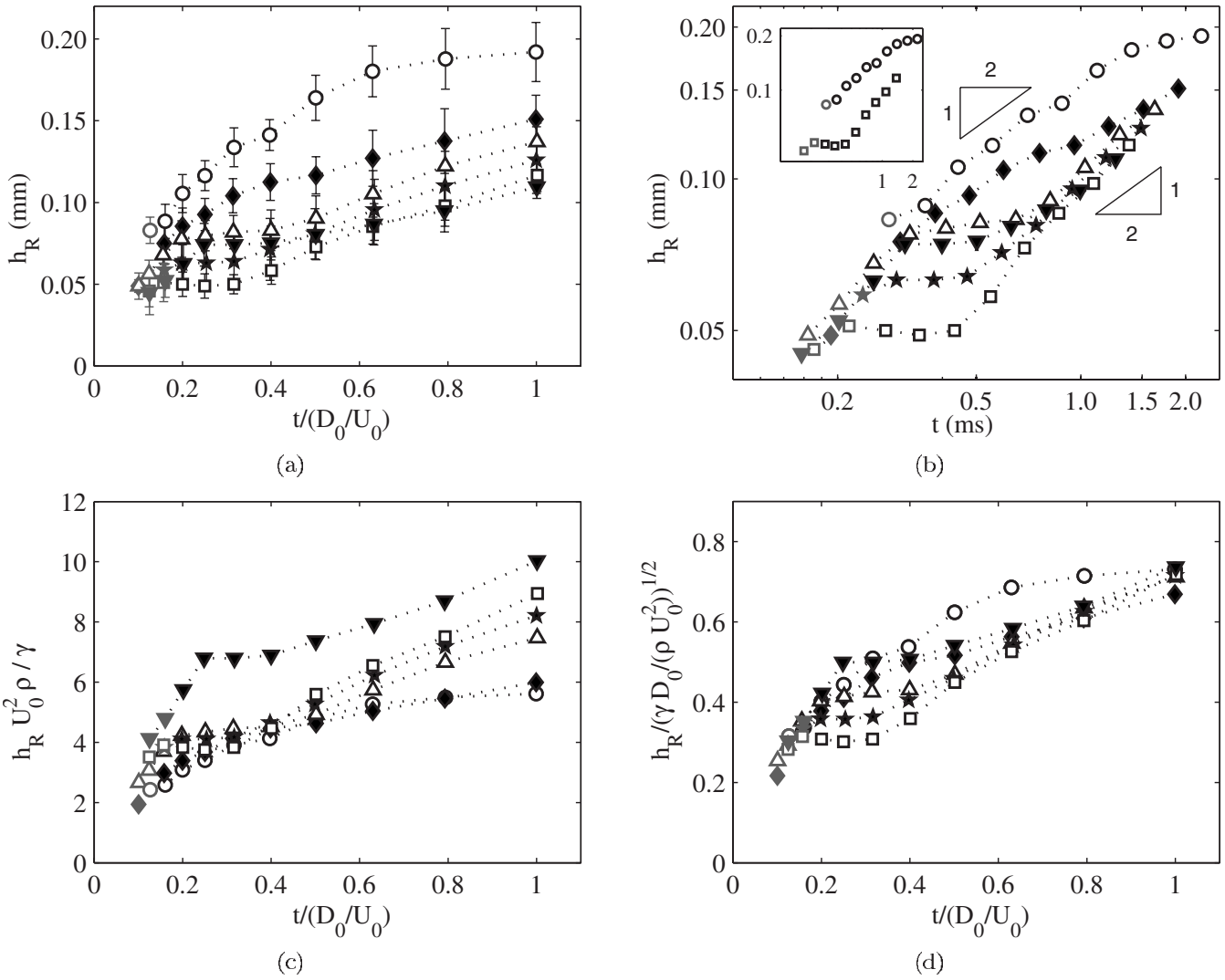


FIG. 3. (a) Rim height, $h_R$, vs dimensionless time after impact, $t/(D_0/U_0)$, for ethanol drops impacting at different impact speeds $U_0$. For the data in parts (a)–(d) we report $U_0$ and (Re/We): (○) 0.91 m/s (1340/59), (♦) 1.06 m/s (1560/80), (△) 1.24 m/s (1820/110), (★) 1.36 m/s (1990/132), (□) 1.47 m/s (2160/154), and (▼) 1.61 m/s (2360/185). The error in the impact speed is ±0.03 m/s. Error bars indicate the 95% confidence interval. Rim heights are measured up to a time $D_0/U_0$ after impact. Dotted lines are drawn to guide the eye. Gray data points are less representative due to the triangular shape of the lamella at early times. (b) Log-log plot of rim thickness, $h_R$, vs time after impact, $t$. The slope of the displayed triangles indicates an approximate square root law (scaling exponent of $\frac{1}{2}$). In parts (b)–(d) error bars have been omitted for clarity but are of the same relative order as in (a). Inset: an example of two impacts taken from the main panel with other data removed for clarity. Note the plateau for the impact of higher speed. (c) Rim height, $h_R$, scaled by $\gamma/(U_0^2\rho)$ vs time after impact, $t/(D_0/U_0)$. (d) Rim height, $h_R$, scaled by $\sqrt{\gamma/(\rho D_0/U_0^2)}$ vs time after impact, $t/(D_0/U_0)$.

### B. Impacts with varying impact speed and constant drop viscosity

We measured the evolution of the rim thickness with time for drops with varying impact speeds and constant drop viscosity. Our results are shown in Fig. 3 and are reported in several formats. Note that in Fig. 3(a) the rim thickness decreases with increasing speed of impact, and that at higher impact speeds the rim thickness displays an unusual plateau behavior at early times. It is possible that the plateau in thickness may be related to the formation of the rim at higher impacts speeds. This interpretation may be relevant as the plateau in thickness spans the time when the outermost portion of the lamella (which we measure) begins to be visibly thicker than the inner portion of the lamella. However, it is intriguing that for the impacts with lower speed no plateau in the thickness is observed although these measurements also span the time of rim development. We are not aware of a previous report of this plateau in rim thickness as the lamella develops. Additionally, the rim thickness is a function of the impact speed, which clearly reveals that the rim thickness is not equivalent to the boundary layer thickness since, traditionally, the boundary layer thickness ($\sqrt{\nu t}$) is invariant with impact speed.

For impacts at high speeds ($U_0 \geq 1.42$ m/s), Roux and Cooper-White[29] fitted their data with a linear increase in thickness in time until a maximum value was reached. However, their lack of spatial resolution makes it difficult to determine the exact form for thickness versus time, particularly at times before $D_0/U_0$. A log-log plot of our data for rim thickness versus time [Fig. 3(b)] and the obtained scaling exponents (Table II), evaluated over the available time interval, suggest that the relationship is not linear. Indeed, it is not

TABLE II. Scaling exponent of the power-law fit of $h_R$ vs $t$ for data in Fig. 3. The scaling exponent is evaluated for a selected region, which encompasses only the region after the plateau for impact speeds $\geq 1.24$ m/s. At low impact speeds the power-law function is fitted for the complete time span up to the characteristic time. Note that these time intervals span only a fraction of a decade and it is, therefore, not clear from our data whether a power-law fit is appropriate.

| Impact speed (m/s) | Selected region (ms) | Scaling exponent (95% confidence interval) |
|---|---|---|
| 0.91 | 0.28–1.40 | $0.50 \pm 0.05$ |
| 1.06 | 0.30–1.91 | $0.36 \pm 0.04$ |
| 1.24 | 0.82–1.63 | $0.6 \pm 0.1$ |
| 1.36 | 0.47–1.49 | $0.63 \pm 0.04$ |
| 1.47 | 0.43–1.37 | $0.7 \pm 0.1$ |
| 1.61 | 0.50–1.26 | $0.4 \pm 0.2$ |

clear from our data whether a power-law fit is appropriate. The time interval between impact and the rim thickness reaching its maximum value spans only a fraction of a decade, making a definitive power-law fit difficult. However, for the reader's interest, and for comparison with previous power-law predictions, we present the best power-law fit to our data in Table II. A $\sqrt{t}$ dependence is consistent with our data for $U_0=0.91$ m/s from shortly after impact until the rim thickness levels off to its maximum value. For higher impact speeds $U_0 \geq 1.24$ m/s an approximate power-law dependence only applies to the time after the plateau behavior, with possible scaling exponents ranging from 0.4 to 0.7. Again, all scaling exponents reported here should be interpreted cautiously as our measurements only span a fraction of a decade in time. However, an approximate $\sqrt{t}$ dependence would only be consistent for low impact speeds up to a time

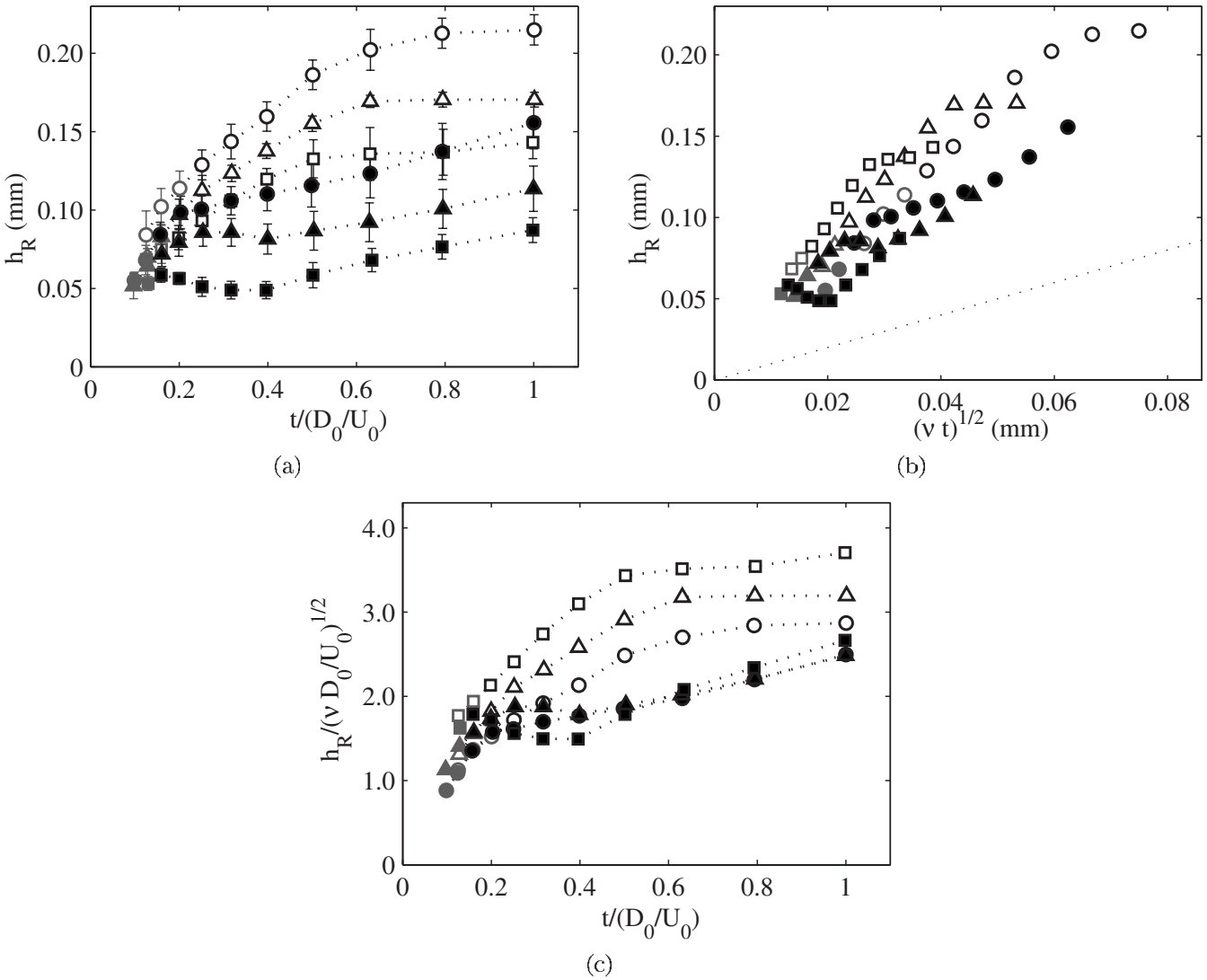


FIG. 4. (a) Rim thickness, $h_R$, vs dimensionless time after impact, $t/(D_0/U_0)$, for drops with varying viscosity (shape of symbols), impacting at two different speeds (open symbols ~0.96 m/s and closed symbols ~1.34 m/s). For the data in parts (a)–(c) we report $\mu$, $U_0$, and (Re/We): (○) 2.05 mPa s, 0.94 m/s (730/64), (△) 1.08 mPa s, 0.98 m/s (1440/69), (□) 0.55 mPa s, 0.95 m/s (2740/62), (●) 2.05 mPa s, 1.36 m/s (1050/135), (▲) 1.08 mPa s, 1.33 m/s (1960/126), and (■) 0.55 mPa s, 1.32 m/s (3810/119). Rim heights are measured up to a time $D_0/U_0$ after impact. Error bars indicate the 95% confidence interval based on five repeated experiments. Dotted lines are drawn to guide the eye. (b) Rim thickness, $h_R$, vs time after impact, scaled according to $\sqrt{\nu t}$. The dotted line represents the function $h=\sqrt{\nu t}$. Error bars have been omitted in parts (b) and (c) for clarity but are of the same relative order as in (a). (c) Rim thickness, $h_R$, scaled by $\sqrt{\nu D_0/U_0}$ vs dimensionless time after impact, $t/(D_0/U_0)$.

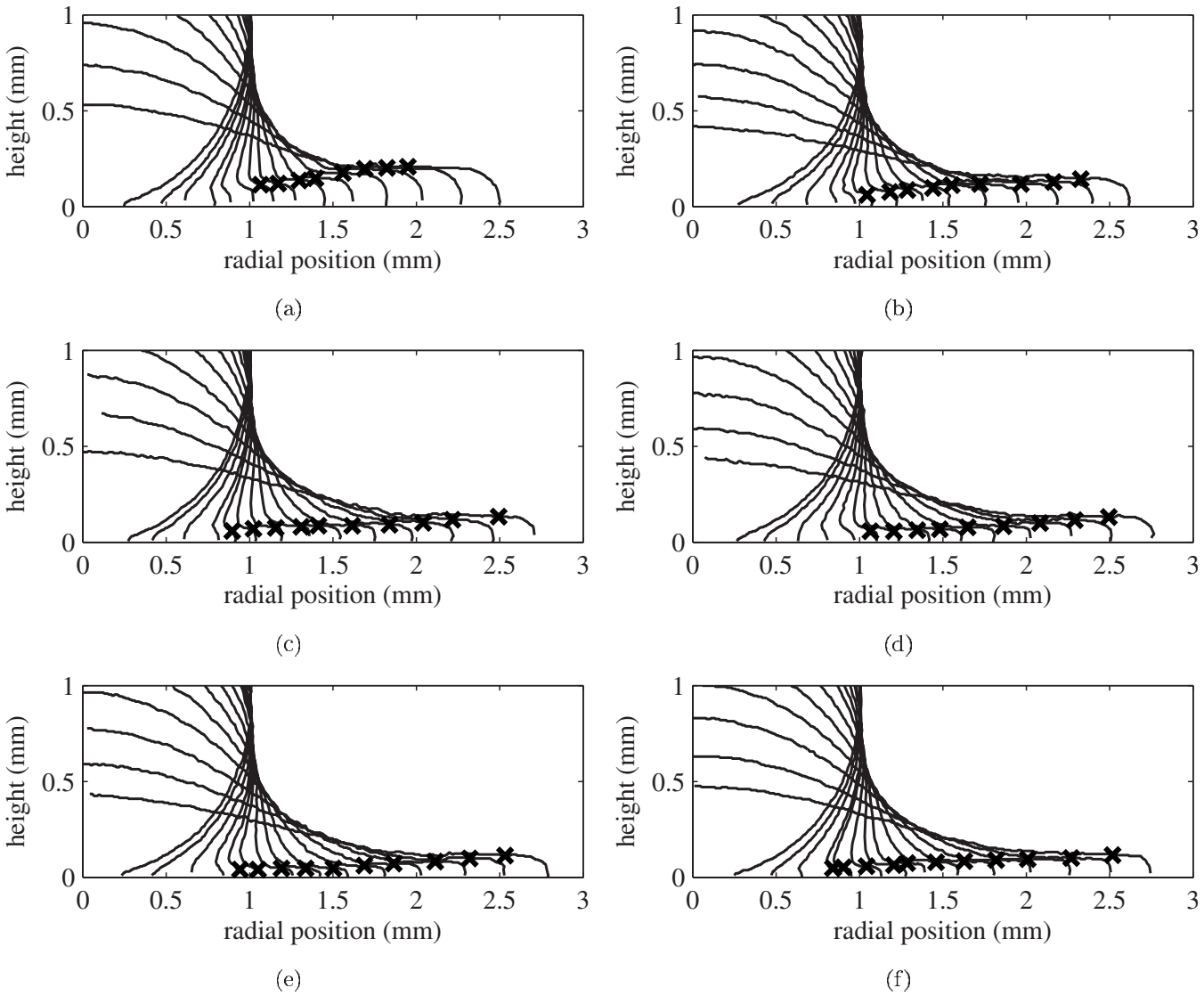


FIG. 5. Height profiles from impacts of ethanol drops with $U_0$= (a) 0.93 m/s, (b) 1.03 m/s, (c) 1.24 m/s, (d) 1.32 m/s, (e) 1.44 m/s, and (f) 1.65 m/s as in Fig. 2(b). Fourteen frames are selected for analysis up to a time $D_0/U_0$ after impact, namely, at 0.004, 0.04, 0.06, 0.10, 0.12, 0.16, 0.20, 0.25, 0.32, 0.40, 0.50, 0.63, 0.79, and 1.00 times $D_0/U_0$.

when the lamella rim has reached a maximum thickness. This result is, perhaps, not surprising as it seems more likely that the rim thickness is set by a competition between surface tension and inertia.

There are two likely length scales that arise from a comparison of surface tension and inertia. The first, $\gamma/(U_0^2\rho)$, comes from directly comparing inertial forces with surface tension forces (i.e., finding the length scale where We=1). The results of scaling the lamella rim by this length are shown in Fig. 3(c). This scaling successfully collapses the two sets of data for low-speed impacts where no plateau behavior occurs. This observation could be coincidental, but if not, it emphasizes that we study behavior that spans two different regimes of behavior—the low-speed impact regime that does not have a plateau, and whose evolution may to some extent be rationalized as a competition of inertial and surface forces, and the high-speed impact regime where a plateau is formed.

The second potential scaling is based on an analogy with the capillary length, $\sqrt{\gamma/(\rho g)}$, but rather than comparing surface tension forces to forces from the vertical acceleration of gravity, $g$, we compare surface tension to forces generated by the rapid deceleration of the lamella in the horizontal direction.[35] We use $U_0^2/D_0$ as an approximation for the horizontal deceleration of the lamella at time $D_0/U_0$, which yields the length scale $\sqrt{\gamma/(\rho D_0/U_0^2)}$. This length scale was previously shown to provide a very good description for the maximum diameter of spreading for drops (mostly on hydrophobic surfaces) with the Weber number comparable to those reported here.[35] The results of scaling the lamella rim by this length are shown in Fig. 3(d). We can see that this collapses the data only at time $t=D_0/U_0$ so it may be a good estimate for the maximum thickness that the lamella reaches during evolution. This idea could be tested by measuring the lamella rim at later times. However, this scaling does not collapse data at earlier times.

Note that at very early times (i.e., in the plateau region)

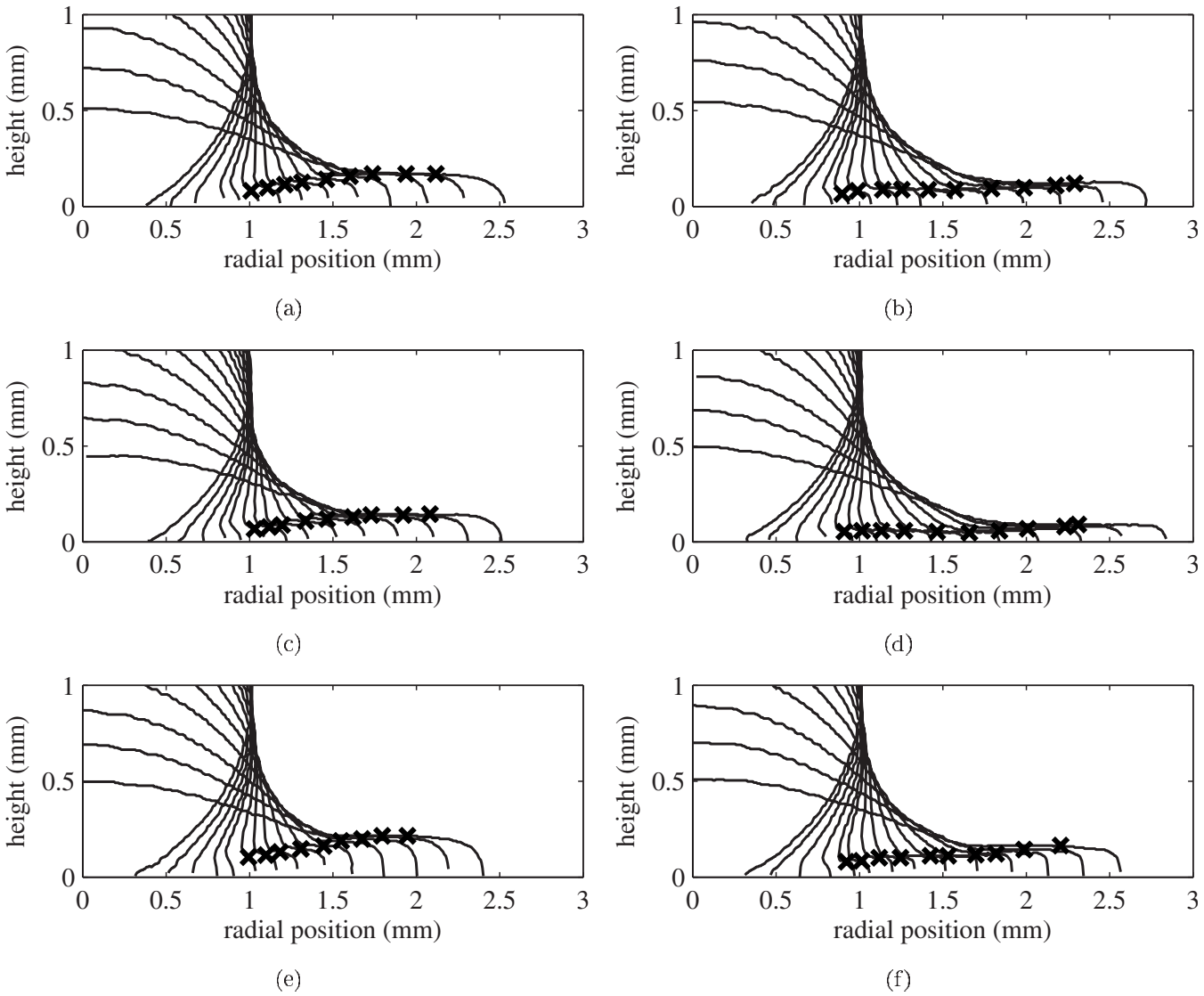


FIG. 6. Height profiles for impacts of drops of (a) ethanol $U_0$=0.97 m/s, (b) ethanol $U_0$=1.36 m/s, (c) methanol $U_0$=0.93 m/s, (d) methanol $U_0$ =1.32 m/s, (e) isopropanol $U_0$=0.92 m/s, and (f) isopropanol $U_0$=1.34 m/s as in Fig. 2(b). Fourteen frames are selected for analysis up to a time $D_0/U_0$ after impact, namely, at 0.004, 0.04, 0.06, 0.10, 0.12, 0.16, 0.20, 0.25, 0.32, 0.40, 0.50, 0.63, 0.79, and 1.00 times $D_0/U_0$.

the highest impact speed ($U_0$=1.61 m/s) has a thicker rim than some of the lower impact speeds. An impact speed of 1.61 m/s is close to the splashing threshold of 1.91 m/s; instabilities may start to form in the lamella, thickening the rim in some areas.

### C. Impacts with varying drop viscosity

The evolution of the rim thickness with time is shown in Fig. 4 for impacting drops of different viscosity. The rim thickness increases with viscosity. For different impact speeds the same trends as in Fig. 3(a) are observed: for each viscosity, a continuously increasing rim thickness is observed at low impact speed, whereas a plateau behavior is observed at high impact speed. Plotting the rim thickness versus $\sqrt{\nu t}$ [Fig. 4(b)] shows that rim thickness is always much larger than the expected boundary layer thickness (dotted line). At low impact speed, $h_R \sim \sqrt{t}$ until the rim thickness levels off to its maximum value (similar to Fig. 3). However, the absence of collapse of the data series obtained at different viscosities shows that rim thickness cannot be described simply by $c\sqrt{\nu t}$, where $c$ is a constant, as the functional dependence on $\nu$ and $U_0$ is more complicated.

To further elucidate the role of viscosity in determining the lamella rim thickness, we show in Fig. 4(c) $h_r$ scaled by the size of the viscous boundary layer at $t=D_0/U_0$. These data again show two distinct regimes for high-speed and low-speed impacts. For the higher speed impacts, the above scaling collapses the data series for times greater than $0.5D_0/U_0$, revealing that viscosity plays a role in the evolution of the lamella at these later times. However, the data series do not collapse for high-speed impacts at earlier times (which are likely the times relevant for the splashing instability[26]), nor do they collapse for the low-speed impacts.

It is also clear from these data that the rim thickness, $h_R$, is dependent on impact speed as, regardless of viscosity, $h_R$ is greater for lower impact speeds. This clear dependence on $U_0$, both here and in Fig. 3, means that those theories of splashing and spreading that scale thickness of the lamella

based on the thickness of a boundary layer (i.e., Refs. 8–11) must be interpreted with caution. In both previous and future scaling arguments related to the lamella it is important to determine which portion of the lamella (inner, rim, or average) should be considered. Some of these theories may use an average lamella thickness or thickness of the inner lamella, which we cannot assess as we do not measure the inner portion of the lamella. For those theories that refer to the rim thickness, it is possible that these theories could be valid for the lamella thickness at times earlier than we can distinguish the existence of a lamella ($\approx 0.07 D_0/U_0$), but as we are uncertain that a lamella exists at these times, it may alternatively be that a boundary layer thickness is important to the flow inside the drop either right before or right after impact. For instance, Mongruel *et al.*[30] suggested that the boundary layer thickness determines the thickness of the lamella when it is initially ejected. In addition, they proposed that the lamella evolution continues to follow a boundary layer thickness up to time $t=(1/\mathrm{Re})(D_0/U_0)\approx 0.2$ $\mu$s for our experiments.[30] However, this time is earlier than the observed time of lamella appearance in both our experiments and those of Mongruel *et al.*

## IV. CONCLUSION

We have measured the evolution of the lamella rim thickness at early times up to $D_0/U_0$, for impact speeds ranging up to the threshold for instabilities to develop in the lamella. At low impact speed, the rim thickness increases approximately with the square root of time, but the dependence on $\nu$ is not a simple square root behavior, leading to a rim thickness consistent with $h_R \approx f(\mu,\rho,U_0,\ldots)\sqrt{t}$ over the limited time range available. In addition to the viscosity and the impact speed, the rim thickness will also likely depend on other parameters such as surface tension and the solid surface properties, which were kept constant in our study. At higher impact speeds we observe a novel behavior: a plateau in thickness at early times. Since high impact speeds are relevant for splashing, this plateau behavior needs to be further investigated. It might be informative to observe simultaneously a top and side view of impact to determine if the plateau behavior is associated with the formation of a thickened rim at the edge of the lamella. The rim thickness is always much larger than the boundary layer thickness and cannot be adequately described by a functional form proportional to $\sqrt{\nu t}$ since the latter does not account for differences in lamella behavior with impact speed $U_0$. Scaling of the rim height using the idea that inertial forces are balanced by capillary pressure gradients provides some collapse of the data at lower impact speeds. Ideally, a full lamella thickness profile as a function of both time after impact and radial distance from the center of the lamella would be measured, but this experiment would be quite challenging.

## ACKNOWLEDGMENTS

We thank James C. Bird and Laurent Courbin for helpful discussions. We also thank the NSF and Harvard MRSEC (Grant No. DMR-0820484) and the NSF IGERT (Grant No. DGE-0221682). Suggestions from the referees are gratefully acknowledged.

## APPENDIX: REPRESENTATIVE HEIGHT PROFILES

Here we give height profiles of one representative impact for each liquid/impact velocity combination reported in Figs. 3 and 4. These results are shown in Figs. 5 and 6. We believe these detailed experimental measurements may be helpful to researchers developing numerical simulations of impact dynamics. Note that the plateau behavior in rim height versus time can be seen in Figs. 5(c)–5(f) and Figs. 6(b), 6(d), and 6(f).

[1] S. Sampath and X. Jiang, "Splat formation and microstructure development during plasma spraying: Deposition temperature effects," Mater. Sci. Eng., A **304–306**, 144 (2001).
[2] J. L. Zable, "Splatter during ink jet printing," IBM J. Res. Dev. **21**, 315 (1977).
[3] D. B. van Dam and C. Le Clerc, "Experimental study of the impact of an ink-jet printed droplet on a solid substrate," Phys. Fluids **16**, 3403 (2004).
[4] M. Gavaises, A. Theodorakakos, and G. Bergeles, "Modeling wall impaction of diesel sprays," Int. J. Heat Fluid Flow **17**, 130 (1996).
[5] W. Wirth, S. Storp, and W. Jacobsen, "Mechanisms controlling leaf retention of agricultural spray solutions," Pestic. Sci. **33**, 411 (1991).
[6] V. Bergeron, D. Bonn, J. Y. Martin, and L. Vovelle, "Controlling droplet deposition with polymer additives," Nature (London) **405**, 772 (2000).
[7] A. L. Yarin, "Drop impact dynamics: Splashing, spreading, receding, bouncing," Annu. Rev. Fluid Mech. **38**, 159 (2006).
[8] C. Josserand, L. Lemoyne, R. Troeger, and S. Zaleski, "Droplet impact on a dry surface: Triggering the splash with a small obstacle," J. Fluid Mech. **524**, 47 (2005).
[9] L. Xu, W. W. Zhang, and S. R. Nagel, "Drop splashing on a dry smooth surface," Phys. Rev. Lett. **94**, 184505 (2005).
[10] I. V. Roisman, K. Horvat, and C. Tropea, "Spray impact: Rim transverse instability initiating fingering and splash, and description of a secondary spray," Phys. Fluids **18**, 102104 (2006).
[11] L. Xu, "Liquid drop splashing on smooth, rough, and textured surfaces," Phys. Rev. E **75**, 056316 (2007).
[12] J. C. Bird, S. Tsai, and H. A. Stone, "Inclined to splash: Triggering and inhibiting a splash with tangential velocity," New J. Phys. **11**, 063017 (2009).
[13] C. Josserand and S. Zaleski, "Droplet splashing on a thin liquid film," Phys. Fluids **15**, 1650 (2003).
[14] S. Chandra and C. T. Avedisian, "On the collision of a droplet with a solid surface," Proc. R. Soc. London, Ser. A **432**, 13 (1991).
[15] C. Mundo, M. Sommerfeld, and C. Tropea, "Droplet-wall collisions: Experimental studies of the deformation and breakup process," Int. J. Multiphase Flow **21**, 151 (1995).
[16] M. Pasandideh-Fard, Y. M. Qiao, S. Chandra, and J. Mostaghimi, "Capillary effects during droplet impact on a solid surface," Phys. Fluids **8**, 650 (1996).
[17] T. Mao, D. C. S. Kuhn, and H. Tran, "Spread and rebound of liquid droplets upon impact on flat surfaces," AIChE J. **43**, 2169 (1997).
[18] I. V. Roisman, E. Berberovic, and C. Tropea, "Inertia dominated drop collisions. I. On the universal flow in the lamella," Phys. Fluids **21**, 052103 (2009).
[19] I. V. Roisman, "Inertia dominated drop collisions. II. An analytical solution of the Navier–Stokes equations for a spreading viscous film," Phys. Fluids **21**, 052104 (2009).
[20] R. D. Schroll, C. Josserand, S. Zaleski, and W. W. Zhang, "Impact of a viscous liquid drop," Phys. Rev. Lett. **104**, 034504 (2010).
[21] I. V. Roisman, R. Rioboo, and C. Tropea, "Normal impact of a liquid drop on a dry surface: Model for spreading and receding," Proc. R. Soc. London, Ser. A **458**, 1411 (2002).
[22] P. Attané, F. Girard, and V. Morin, "An energy balance approach of the dynamics of drop impact on a solid surface," Phys. Fluids **19**, 012101 (2007), in particular, see p. 012101-9, col. 2, for a discussion of the regime of model validity.
[23] K. F. Loehr and A. Lasek, "Splashing of drops," Arch. Mech. **42**, 507 (1990).

[24]S. T. Thoroddsen and J. Sakakibara, "Evolution of the fingering pattern of an impacting drop," Phys. Fluids **10**, 1359 (1998).
[25]R. Rioboo, C. Tropea, and M. Marengo, "Outcomes from a drop impact on solid surfaces," Atomization Sprays **11**, 155 (2001).
[26]R. E. Pepper, L. Courbin, and H. A. Stone, "Splashing on elastic membranes: The importance of early-time dynamics," Phys. Fluids **20**, 082103 (2008).
[27]L. Xu, L. Barcos, and S. R. Nagel, "Splashing of liquids: Interplay of surface roughness with surrounding gas," Phys. Rev. E **76**, 066311 (2007).
[28]C. D. Stow and M. G. Hadfield, "An experimental investigation of fluid flow resulting from the impact of a water drop with an unyielding dry surface," Proc. R. Soc. London, Ser. A **373**, 419 (1981).
[29]D. C. D. Roux and J. J. Cooper-White, "Dynamics of water spreading on a glass surface," J. Colloid Interface Sci. **277**, 424 (2004).
[30]A. Mongruel, V. Daru, F. Feuillebois, and S. Tabakova, "Early post-impact time dynamics of viscous drops onto a solid dry surface," Phys. Fluids **21**, 032101 (2009).
[31]H.-Y. Kim, Z. C. Feng, and J.-H. Chun, "Instability of a liquid jet emerging from a droplet upon collision with a solid surface," Phys. Fluids **12**, 531 (2000).
[32]P. D. Nikam, T. R. Mahale, and M. Hasan, "Density and viscosity of binary mixtures of ethyl acetate with methanol, ethanol, propan-1-ol, propan-2-ol, butan-1-ol, 2-methylpropan-1-ol, and 2-methylpropan-2-ol at (298.15, 303.15, and 308.15) K," J. Chem. Eng. Data **41**, 1055 (1996).
[33]G. Vázquez, G. Antorrena, J. M. Navaza, and V. Santos, "Absorption of $CO_2$ by water and surfactant solutions in the presence of induced Marangoni effect," Chem. Eng. Sci. **51**, 3317 (1996).
[34]Y. Renardy, S. Popinet, L. Duchemin, M. Renardy, S. Zaleski, C. Josserand, M. A. Drumright-Clarke, D. Richard, C. Clanet, and D. Quéré, "Pyramidal and toroidal water drops after impact on a solid surface," J. Fluid Mech. **484**, 69 (2003).
[35]C. Clanet, C. Béguin, D. Richard, and D. Quéré, "Maximal deformation of an impacting drop," J. Fluid Mech. **517**, 199 (2004), see, in particular, p. 202.